Materials Today Bio 24 (2024) 100890

Contents lists available at ScienceDirect

Materials Today Bio

journal homepage: www.journals.elsevier.com/materials-today-bio

Injectable Microparticle-containing hydrogel with controlled release of bioactive molecules for facial rejuvenation

Semi Lee [a,1], Seung-Woon Baek [a,b,c,1], Da-Seul Kim [a], So-Yeon Park [a,d], Jun Hyuk Kim [a], Ji-Won Jung [a], Jun-Kyu Lee [a], Gi-Min Park [a], Chun Gwon Park [b,c], Dong Keun Han [a,*]

[a] Department of Biomedical Science, CHA University, 335 Pangyo-ro, Bundang-gu, Seongnam-si, Gyenggi 13488, South Korea
[b] Department of Biomedical Engineering, SKKU Institute for Convergence, Sungkyunkwan University (SKKU), 2066 Seobu-ro, Jangan-gu, Suwon-si, Gyenggi 16419, South Korea
[c] Department of Intelligent Precision Healthcare Convergence, SKKU Institute for Convergence, Sungkyunkwan University, 2066 Seobu-ro, Jangan-gu, Suwon-si, Gyenggi 16419, South Korea
[d] Division of Biotechnology, College of Life Sciences and Biotechnology, Korea University, Seoul 02841, South Korea

ARTICLE INFO

Keywords:
Skin regeneration
Rejuvenation
HA hydrogel
PLLA microparticle
Inorganic particle
Asiaticoside

ABSTRACT

The skin is the largest organ and a crucial barrier for protection against various intrinsic and extrinsic factors. As we age, the skin's components become more vulnerable to damage, forming wrinkles. Among different procedures, hyaluronic acid-based hydrogel has been extensively utilized for skin regeneration and reducing wrinkles. However, it has limitations like low retention and weak mechanical properties. In this study, we suggested the poly(L-lactic acid) (PLLA) microparticles containing alkaline magnesium hydroxide and nitric oxide-generating zinc oxide and rejuvenative hyaluronic acid (HA) hydrogels including these functional microparticles and asiaticoside, creating a novel delivery system for skin rejuvenation and regeneration. The fabricated rejuvenative hydrogels have exhibited enhanced biocompatibility, pH neutralization, reactive oxygen species scavenging, collagen biosynthesis, and angiogenesis capabilities *in vitro* and *in vivo*. Additionally, an excellent volume retention ability was demonstrated due to the numerous hydrogen bonds that formed between hyaluronic acid and asiaticoside. Overall, our advanced injectable hydrogel containing functional microparticles, with controlled release of bioactive molecules, has a significant potential for enhancing the regeneration and rejuvenation of the skin.

1. Introduction

The skin is the largest organ in the body and functions as an essential protective barrier against microorganisms and dehydration. However, with age, the skin becomes more vulnerable to damage [1,2] due to decreased fibroblasts and extracellular matrix (ECM) components, leading to wrinkles, volume depletion, and sagging skin [3]. In addition, an inflammatory response can expedite skin senescence and induce apoptosis [4]. Therefore, it is essential to inhibit inflammatory response and stimulate angiogenesis for skin repair and regeneration [5,6]. In biomedical applications leading to skin regeneration, hyaluronic acid (HA)-based hydrogels have gained significant attention due to their biocompatibility, biodegradability, and ease of chemical modification [7–9]. In cosmetology, HA dermal filling agents are commonly used for facial rejuvenation, offering non-invasive and minimally traumatic options [3]. However, HA-based hydrogels have limitations, such as rapid degradation, poor long-term mechanical properties, and a short half-life. Several studies enhanced the durability and mechanical strength of HA. You et al. fabricated copper/tannic acid nanosheets with a cross-linked matrix of alginate and gelatin and had an elongated retention time [10]. Sallstrom et al. reported that laponite, a nano-composite synthesized by hectorite nano clay, was loaded with HA and manufactured by a printing-then-curing approach [11]. Abu-Hakmeh et al. suggested sequential gelation by oxidative reaction of hydrogen peroxide (H_2O_2) and horseradish peroxidase (HRP) to increase mechanical strength [12]. However, despite chemical cross-linking and enzymatic modifications, the duration of HA in the body remains shorter [13].

To address this issue, biodegradable polymer microspheres improved

* Corresponding author.
E-mail address: dkhan@cha.ac.kr (D.K. Han).
[1] These authors contributed equally to this work.

https://doi.org/10.1016/j.mtbio.2023.100890
Received 18 October 2023; Received in revised form 20 November 2023; Accepted 28 November 2023
Available online 1 December 2023

the longevity of cross-linked HA fillers [14,15]. Among these biodegradable polyesters, poly(L-lactic acid) (PLLA), FDA-approved for medical devices, exhibited a slow degradation rate due to its semi-crystalline and hydrophobic characteristics [16]. Nevertheless, when PLLA was implanted in the body, it generated acidic byproducts of lactic acid hydrolysis, leading to tissue inflammation and necrosis [17]. Magnesium hydroxide (MH) was utilized to overcome these limitations due to nontoxic inorganic particles that have a pH-neutralizing effect on acidic byproducts and could suppress the inflammatory response [18–21].

Nitric oxide (NO) is an endogenously synthesized signaling molecule primarily produced by nitric oxide synthase (eNOS) in endothelial cells, playing critical physiological roles in regulating and regenerating numerous tissues and organs [22]. In the dermal microenvironment, NO promotes collagen biosynthesis and wound healing by enhancing angiogenesis [23]. Several studies have demonstrated that NO can be generated by enzyme-mimic catalysis activity in metals and metal oxides, with zinc oxide (ZO) displaying the most significant generation effects [24]. ZO continuously generates NO by a redox reaction with NO donor in the presence of blood making it the subject of interest in various fields, including biotechnology, medicine, biology, and physics [25]. Moreover, NO generated from ZO in the dermal region plays an essential role in wound repair, participating in an inflammatory response, angiogenesis, and collagen production [23,26].

Asiaticoside (ATS) is a triterpenoid compound isolated from *Centella asiatica*, and it has been clinically proven to stimulate wound healing and skin regeneration by promoting collagen synthesis, angiogenesis, and cell proliferation [27]. ATS stimulates fibroblasts, forming collagen and elastin, and it also activates the TGF-β receptor I kinase-independent Smad pathway, inducing type 1 collagen synthesis [2].

In this study, poly(L-lactide) (PLLA) microparticles (PMZ) loaded with functional inorganic particles, such as surface-modified magnesium hydroxide and zinc oxide, that inhibit inflammation, and produce NO for a prolonged period through dual mechanisms, respectively were prepared. A rejuvenating hydrogel incorporating microparticles and ATS was developed with a sustained release system. *In vitro* experiments were conducted to verify the biocompatibility and anti-inflammatory effects in human dermal fibroblasts (hDFs) and human umbilical vein endothelial cells (HUVECs). Additionally, the hydrogel was implanted into the dermal region of mice for 16 weeks to evaluate angiogenesis, collagen formation, and volume retention ability *in vivo*.

2. Materials and methods

2.1. Materials

Poly(L-lactide) (PLLA, Mw 240 kDa) was procured from Green Chemical (Korea). Polyvinyl alcohol (PVA), magnesium hydroxide [Mg $(OH)_2$; MH], oleic acid (OA), zinc oxide [(ZnO); ZO], α-lipoic acid (ALA), glutathione (GSH), and S-nitroso-N-acetyl-DL-penicillamine (SNAP) were purchased from Sigma-Aldrich (USA). The cross-linked hyaluronic acid hydrogel with divinyl sulfone (DVS) was provided by BioPlus Co., Ltd (Korea). Dichloromethane (DCM) was obtained from Daejung Co. Ltd. (Korea). Asiaticoside (ATS), 4-amino-5-methylamino-2′,7′-difluorofluorescein diacetate (DAF-FM DA), 2,2-diphenyl-1-(2,4,6-t2,4,6-trinitrophenolzyl (DPPH), and 2′, 7′-dichlorofluorescein diacetate (DCF-DA) were purchased from Cayman Chemical (USA). Human dermal fibroblasts (hDFs) were purchased from the American Type Culture Collection (PCS-201-012, ATCC, USA). Human umbilical vein endothelial cells (HUVECs) and EGM-2 media were purchased from Lonza (Switzerland). Dulbecco's Modified Eagle Medium (DMEM), fetal bovine serum (FBS), and phosphate-buffered saline (PBS) solution were purchased from Hyclone (USA). The Universal RNA Extraction Kit was purchased from Bioneer (Korea). The antibiotic antimycotic solution (AA), TRIzol reagent (15596018), SYBR Green PCR Master Mix (Applied Biosystems), Live/Dead staining Kit (Calcein AM/EthD-1), and Pierce™ BCA Protein Assay Kit were obtained from Gibco (Thermo Fisher Scientific, USA). Cell-count Kit (CCK-8) was obtained from Dongin LS (Korea). PrimeScript RT Reagent Kit (Perfect Real Time) was purchased from Takara (Japan).

2.2. Preparation and characterization of pH neutralized and NO-generating microparticles

MH was surface modified with oleic acid to enhance its dispersity and stability within the hydrophobic polymer matrix (MO). MH (3 g) was added to 70 mL hexane with OA (750 mg). The mixture was reacted at 70 °C for 4 h under stirring. The unreacted OA was removed by centrifugation. The ZO was conjugated with ALA to improve dispersity, stability, and NO generating ability, as in our previous study (ZA) [25]. The ZO (1.5 g) was added to 50 mL chloroform with 1.5 g ALA and reacted at 60 °C for 24 h with continuous stirring. The unreacted ALA was eliminated by centrifugation. The size distribution of synthesized MO and ZA was analyzed by dynamic laser scattering (DLS; Malvern, UK). The attenuated total reflection-Fourier transform infrared spectroscopy (ATR-FTIR; PerkinElmer, USA) was used to investigate the specific chemical structure of the MO and ZA within the range between 600 and 4000 cm^{-1} with a resolution of 4 cm^{-1} over 32 scans. The combined ratio of the MO and ZA was estimated by thermogravimetric analysis (TGA; PerkinElmer, USA).

The pH neutralized and NO-generating microparticles were fabricated by the oil-in-water emulsion solvent evaporation method. A discontinuous phase solution was prepared by adding 40 mg MO and 20 mg ZA to 10 mL DCM in which 200 mg PLLA were dissolved, and a continuous phase solution was prepared by dissolving 2 % (w/v) PVA in deionized water. The discontinuous and continuous phase solutions were mixed and homogenized at 1500 rpm for 3 min (Silverson Machines Ltd, U.K.). An evaporator (N–1300, Eyela, Japan) was used to remove DCM from the emulsion for 60 min under a vacuum. The PLLA microparticles were harvested with a size of less than 25 and 75 mm using a sieve and washed by centrifugation at 3500 rpm for 10 min.

Surface morphology and element mapping of functional microparticles were visualized using scanning electron microscopy (SEM; S-4800, HITACHI, Japan). The sizes distribution of microparticles was measured using Laser Diffraction (Mastersizer 2000, Malvern Instruments Ltd, UK). The ratio of inorganic particles within the functional microparticles was analyzed by TGA. The release amounts magnesium and zinc in the functional microparticles was measured by inductively coupled plasma-optical emission spectroscopy (ICP-OES, Optima 8000, Perkin Elmer, MA, USA). The sustainability of NO generated by microparticles was investigated using a DAF-FM DA fluorescent probe and chemiluminescence nitric oxide analyzer (NOA; Sievers NOA 208i, GE Analytical Instrument, USA). The microparticles (10 mg) were immersed in PBS solution for 7 days. Fluorescent images were visualized using a fluorescent-labeled organism bioimaging instrument (FOBI; CellgenTEK Co., Korea) with 50 μM DAF-FM DA, 50 μM GSH, and 50 μM SNAP at 37 °C for 2 h, and quantitative fluorescence intensity was measured by irradiating excitation (λ_{max} 495 nm) and emission (λ_{max} 515 nm) frequencies.

2.3. Preparation and characterization of rejuvenative hydrogels containing functional microparticles

ATS (500 μg) was dispersed in 40 μL PBS solution and blended with 60 μL hydrogel and 2 % microparticles. FE-SEM analysis was performed to observe the distribution and morphology of microparticles in the hydrogels and freeze-dried before the measurement. The rheological properties of hydrogels were analyzed using a strain-controlled rheometer, ARES-G2 (SN#4010-0255, TA Instrument, USA) with a frequency range of 0.1–10 Hz at 25 °C. The hydrogels were filled in a 1 mL syringe equipped with a 26 G needle, and injectable force was measured using a universal testing machine (UTM; T0-101, TEST ONE, Korea) at a flow rate of 30 mm/min. To investigate the release behavior of ATS, 150 μL

sample was immersed in 3 mL PBS solution at 37 °C for 28 days, and the supernatant was collected. The released ATS amount was determined with high-performance liquid chromatography (HPLC, LC 1100, Agilent, Germany) with an Agilent Eclipse column (5 μm, 4.6 × 150 mm C-18). The mobile phase consisted of acetonitrile, water, and methanol (57:38: 5) with a 1 mL/min flow rate. The sample injection volume was 10 μL and the UV detection wavelength was 217 nm for 2 min.

2.4. Evaluation of cell proliferation

hDFs and HUVECs were cultured in DMEM media and EGM-2 media bullet Kit supplemented with 10 % FBS and 1 % AA, respectively. Both cells were grown under a humidified atmosphere at 37 °C with 5 % CO_2. The hDFs (1×10^4 cells/well) and HUVECs (3×10^4 cells/well) were seeded in a 24-well plate, and 30 μL/mL hydrogels were placed in each well with indirect diffusion technique using 24-well inserts, respectively. Some wells seeded with HUVECs were additionally treated with 10 μM GSH and 10 μM SNAP at 0 and 12 h. After 24 h, cell proliferation was measured using a Live/Dead (Calcein AM/EthD-1) staining Kit and CCK-8 following the manufacturer's instructions. An LSM880 (Zeiss, Germany) was used to obtain the Live-Dead fluorescent images.

2.5. ROS scavenging effect

Prior to use, DPPH (0.25 mM) was dissolved in 95 % ethanol. Subsequently, 100 μL hydrogel was added into 1 mL DPPH solution and shaded from the light for 24 h under gentle shaking. The absorbance was measured using a SpectraMax M2 Microplate Reader (Molecular Devices, USA). The hDFs were seeded onto 24-well plates and treated with an indirect diffusion technique. The generated reactive oxygen species (ROS) from the cells was visualized using 20 μM DCF-DA for 45 min at 37 °C, and the nuclei of cells were stained using Hoechst. Each well was washed with PBS solution 2 times and DCF-DA positive cells were imaged using fluorescence microscopy.

2.6. RNA extraction and quantitative real-time PCR

The cells (hDFs and HUVECs: 2×10^5 cells/well) were seeded into a 6-well plate and hydrogels were placed in each well using 6-well inserts. Total cellular RNA was extracted using Universal RNA Extraction following the manufacturer's instructions. Extracted RNA concentration was determined by a spectrophotometer and reverse-transcribed to complementary DNA using PrimeScript RT Reagent Kit following the documentation provided. qRT-PCR was carried out using each primer set and SYBR Green PCR Master Mix and a QuantStudio 3 real-time PCR (Applied Biosystems, USA) instrument. The expression of gene values was normalized with the 18s rRNA and calculated using the $2^{-\Delta\Delta Ct}$ method. The following primer sequences (forward; reverse) were used:

18s: 5′-cctggataccgcagctagga-3′; 5′-gcggcgcaatacgaatgcccc-3′

SOD-1 (superoxide dismutase-1): 5′-aaacctcagccctaacggtg-3′; 5′-acatcaatcccagcagtgg-3′

CAT (catalase): 5′-gaccactggagctggtaacc-3′; 5′-ctgtgtcagctgaacccgat-3′

BAK (BCL-2 antagonist-1): 5′-agacctgaaaaatggcttcg-3′; 5′-cggaaaacctcctctgtgtc-3′

BCL2 (B-cell lymphoma protein-2): 5′-agtacctgaaccggcacct-3′; 5′-gccgtacagttccacaaagg-3′

P16 (tumor suppressor gene P16): 5′-ctactgaggagccagcgtcta-3′; 5′-ctgcccatcatcatgacct-3′

P53 (tumor suppressor gene P53): 5′-ccctttttggacttcaggtg-3′; 5′-aggccttggaactcaaggat-3′

COL1A1 (collagen type 1): 5′-gggattccctggacctaaag-3′; 5′-ggaacacctcgctctcca-3′

COL3A1 (collagen type 3): 5′- gctaaccttgatgctataactacga-3′; 5′-tggtggtaaaggcgaaatg-3′

MMP1 (matrix metallopeptidase1): 5′-gctaaccttgatgctataactacga-3′; 5′-tttgtgcgcatgtagaatctg-3′

Elastin: 5′-ttggagttggtgctggtgtt-3′; 5′-gctgctccatatttggctgc-3′

TGF-β (transforming growth factor-β): 5′-gacttttccccagacctcgg-3′; 5′-ataggggatctgtggcaggt-3′

α-SMA (α-smooth muscle actin): 5′-gaagaggacactgcctt-3′; 5′-tcccagttggtgatgatgcc-3′

HIF-1α (hypoxia-inducible factor-1α): 5′-tttttcaagcagtaggaatt-3′; 5′-gtgatgtagtagctgcatga-3′

eNOS (endothelial nitric oxide synthase): 5′-atccagtgccctgcttca-3′; 5′-gcagggcaagttaggatcag-3′

VEGF (vascular endothelial growth factor): 5′-actggaccctggctttactg-3′; 5′-tctgctccccttctgtcgt-3′

ANGPT1 (angiopoietin 1): 5′-tccacataggaaatgaaaagca-3′; 5′-cagcaccgtgtaagatcagg-3′

IL-6 (interleukin-6): 5′-gatgagtacaaaagtcctgatcca-3′; 5′-ctgcagccactggttctgt-3′

IL-8 (interleukin-8): 5′-agacagcagagcacacaagc-3′; 5′-atggttccttccggtggt-3′

IL-1β (interleukin-1β) 5′-tacctgtcctgcgtgttgaa-3′; 5′-tctttgggtaatttttgggatct-3′

COX-2 (cyclooxygenase-2): 5′-gcaattattccccatgaacg-3′; 5′-gggacttaatcaacgcaagc-3′

2.7. Collagen biosynthesis capability evaluation

Western blot was performed to investigate the expression of collagen biosynthesis-related protein. The cells were rinsed with PBS solution 2 times and lysed at 4 °C using RIPA lysis buffer. The lysates were vortexed and incubated at 4 °C for 30 min and finally centrifuged at 13,000 rpm for 10 min at 4 °C. The protein concentration was determined using the Pierce™ BCA Protein Assay Kit. The proteins were cooked with 4x Laemmli sample buffer at 105 °C. The samples were loaded onto a 10 % SDS-PAGE gel and transferred to nitrocellulose membranes. The membranes were blocked with 5 % skim milk (BD Difco, USA) in TBST (Tris-buffered saline with Tween-20). Primary antibody, COL1A1 (sc-59772, Santa Cruz, Biotechnology, USA, 1:200 dilution), and GAPDH (5174T, Cell signaling Technology, USA, 1:1000 dilution) were incubated overnight at 4 °C on the membranes. After 24 h, the membranes were washed in TBST for 30 min and labeled with anti-mouse (7076S, Cell signaling Technology, USA, 1:5000 dilution) and anti-rabbit (7074P2, Cell signaling Technology, USA, 1:5000 dilution). Finally, the immunoreactivity was assessed with the ECL Select™ Luminal Solution (Cytiva, USA).

The expression of collagen biosynthesis-related protein was visualized to immunocytochemistry analysis. The hDFs were planted at a density of 3×10^4 cells on a 24-well plate and the PLLA hydrogels were treated. After 24 h, the cells were washed with PBS solution, fixed with 4 % PFA solution for 15 min, permeabilized with 0.3 % triton for 30 min, and finally blocked by 1 % BSA solution for 30 min. Cells were probed with a COL1A1 antibody (Santa Cruz Biotechnology, USA) in 5 % BSA/0.1 % Triton X-100 solution at 4 °C overnight. After rinsing with PBS solution and treated secondary antibody (Alexa-Fluor 568 goat anti-rabbit; Molecular Probes Inc., USA) in 5 % BSA/0.1 % Triton X-100 for 1 h at room temperature. Following 3 times washed with PBS solution and mounted using Vectashield mounting medium/DAPI (Vector, USA). The cells were visualized using fluorescence microscopy.

2.8. Angiogenic ability assessment

To verify the migration of HUVECs by hydrogel, the cells were cultured in 6-well plates at a density of 1×10^4 cells until a confluent monolayer. The grown cells were scratched with a sterilized 1 mL micropipette tip and washed using PBS solution 2 times to remove cell debris. Also, hydrogels were treated using 6-well inserts with 10 μM GSH and 10 μM SNAP. After 14 h, each well was observed using an optical microscope (CKX53, Olympus, Japan). The wound closure area was

quantified using NIH Image J software (National Institutes of Health, USA) and calculated as a percentage compared to the area of the initial wound.

To evaluate the angiogenic ability of PLLA hydrogels in HUVECs, 250 μL Matrigel matrix (356234, Corning) was coated on a 24-well plate at 37 °C incubator for 1 h [22]. The cells (1.2×10^5 cells per well) were grown for 16 h onto a Matrigel matrix. After 16 h, the cells were stained with 4 μM Calcein AM and incubated for 15 min. The formed tube was visualized by fluorescence microscopy and quantified using by NIH Image J software.

2.9. Animals and histological evaluation

The animal experimental protocols were evaluated and approved by the Institutional Animal Care and Use Committee of CHA University (IACUC230122). The mice used in the study were 8-week-old (BALB/C, Orient Bio Inc., Korea). The mice were anesthetized with 2 % isoflurane (TerrellTM Isoflurane, Piramal Critical Care Inc., USA). Following shaving, 100 μL of hydrogels were injected into the left and right dorsal regions of the subcutaneous tissue using 26 G needles. After 4, 8, and 16 weeks, mice were sacrificed and evaluated. The tissues were fixed in 4 % paraformaldehyde for 3 days and embedded in paraffin. The paraffin cross-sectioned to 5 μm thickness was stained with Hematoxylin and Eosin (H&E) and Masson's Trichrome (MT; VitroVivo Biotech, USA) following the manufacturer's instructions. mRNA was isolated using TRIzol reagent from the tissue of mice, and reverse-transcribed to complementary DNA using PrimeScript RT Reagent Kit following the documentation provided. qRT-PCR was carried out using each primer set and SYBR Green PCR Master Mix. The expression of gene values was normalized with the 18s rRNA and calculated using the $2^{-\Delta\Delta Ct}$ method. The following primer sequences (forward; reverse) were used: 18s (5′-gccgctagaggtgaaattctt-3′; 5′-cgtcttcgaacctccgact-3′), interleukin-6 (IL-6; 5-acggccttccctacttcaca-3′; 5′-catttccacgatttcccaga-3′), interleukin-1β (IL-1β; 5′-agttgacggaccccaaaag-3′; 5′-agctggatgctctcatcagg-3′), collagen type 1 (COLA1A; 5′-ttctcctggcaaagacggac-3′; 5′-ttctcctggcaaagacggac-3′), collagen type 3 (COL3A1; 5′-cagccaggtcgagatggatc-3′; 5′-gccacgttcac-cagtttcac-3′), Elastin (5′-aaatatggtgctgctggcct-3′; 5′-ctcttccggccacaggattt-3′), α-smooth muscle actin (α-SMA; 5′-tggacgggatctcacagact-3′; 5′-gaagcgctcgttgccaatag-3′), hypoxia-inducible factor-1α (HIF-1α; 5′-caggctgctgtaacgatgaa-3′; 5′-ctctatccacatcaaagcaa-3′), angiopoietin 1 (ANGPT-1; 5′-ggaagatggaagcctggat-3′; 5′-accagagggattcccaaaac-3′), vascular endothelial growth factor (VEGF; 5′-caggctgctgtaacgatgaa-3′; 5′-gctttggtagggtttgatcc-3′). Immunofluorescence staining was performed with anti-CD31 (ab28364, Abcam 1:500) and VCAM-1 (sc-13160, Santa Cruz Biotechnology, USA, 1:100) as primary antibodies (4 °C overnight), and Alexa Fluor 488 and 555 (1:200) secondary antibodies. After staining the nuclei with Hoechst, the images were acquired through confocal microscope (Leica TCSSP5II, Germany).

2.10. Statistical analysis

All experiments were repeated at least three times. The results are shown as the means ± SD. Statistically significant differences were evaluated by one-way ANOVA with post hoc analysis (Tukey method) using GraphPad Prism 7.0 software (GraphPad Software Inc., USA). #$p < 0.0001$, ***$p < 0.001$, **$p < 0.01$, and *$p < 0.05$ were regarded as statistically significant differences.

3. Results and discussion

3.1. Characterization of pH neutralized and NO-generating microparticles

As mentioned previously, MH has the ability to pH-neutralize acidic by-products of polyester. However, hydrophilic inorganic particles such as MH and ZO have poor dispersibility and stability in organic solvents and polyester matrices. To improve dispersibility, many approaches have been reported for the surface modification of inorganic particles using stearic acid, ricinoleic acid, and silane [28–30]. Herein, the MH was surface-modified with OA as a hydrophobic substance to synthesize MO nanoparticles. The characterization of the MO is shown in Fig. S1. Outstanding dispersibility in organic solvent was exhibited in MO compared to the immediate precipitation of MH (Fig. S1A). The size of MO in the organic solvent was 358.7 ± 3.3 nm, and MH was precipitated in size larger than micro, making it impossible to measure (Fig. S1B). To demonstrate that MH and OA were chemically bonded, FTIR and TGA were performed. In Fig. S1C, O–H stretching vibration (3270 cm^{-1}) derived from MH and symmetric, asymmetric stretching (C–H), and a carbonyl group (C═O) (2923, 2854, and 1708 cm^{-1}, respectively) derived from OA were observed in FTIR spectrum of MO [31,32]. The conjugation ratio of OA on the MH surface was quantified at 3.65 % through TGA analysis (Fig. S1D).

As in our previous study, ZO was conjugated with ALA by a bidentate chelating reaction to synthesize ZA nanoparticles with NO-generating increased by combination of two generative mechanisms and improved dispersibility [25]. The ZA was highly dispersible in organic solvent and had a size of 118.8 ± 5.2 nm (Figs. S2A and B). Asymmetric stretching (C–H), symmetric stretching (C–H), carbonyl group (C═O), and O–H stretching (2927, 2865, 2844, and 3468 cm^{-1}, respectively) derived from ZO and ALA were detected in the FTIR spectrum of ZA, with 8.92 % ALA bound in the ZA (Figs. S2C and D) [33,34].

The prepared surface-modified inorganic nanoparticles (MO and ZA) were loaded in PLLA microparticles by an oil-in-water emulsion solvent evaporation method to fabricate MO-containing (PM) and MO/ZA-containing (PMZ) PLLA microparticles (Scheme 1). The morphology of pH neutralized and NO-generating microparticles and the distribution of surface-modified inorganic nanoparticles within them were visualized using SEM and EDS mapping (Fig. 1A). The functional microparticles had spherical in shape comparative uniform size. The Mg element mapping shown in PM and PMZ and the Zn element mapping shown in PMZ were detected in the same shape as microparticles, which means that MO and ZA are evenly spread in the particles. In general, the size of microparticles injected subcutaneously is limited to more than 40 μm because it can induce capillary embolism, whereas large-sized particles can cause foreign body sensation [35]. Therefore, the functional microparticles were prepared with the oil-in-water emulsion-solvent evaporation method and harvested using sieve within 45–50 μm. The sizes of PLLA, PM, and PMZ were 45 ± 0.04, 49.88 ± 0.14, and 49.58 ± 0.36 μm, respectively (Fig. 1B). The MH and ZO loading amounts in functional microparticles were measured by TGA and ICP-OES analysis (Fig. 1C and Table S1). The MH loading ratio of PM microparticles was 22.83 % ± 0.51 when calculated considering the molecular weight decrease during thermal decomposition [35]. The ratio of the thermal decomposition products of PMZ was 25.77 % ± 0.89. The ratio of MH to ZO in PMZ was unknown because MH is thermally decomposed, whereas ZO is not. The exact ratio of MH and ZO in the PMZ was investigated by ICP-OES. The amounts of MH and ZO within PMZ were 231.14 ± 5.17 (23.11 %) and 108.19 ± 4.64 μg/mg (10.82 %), respectively, and these results are consistent when compared with the thermogram of PMZ. The loading efficiency of MH and ZO within the functional microparticles was 104.38 % and 101.27 %, respectively.

The real-time catalytic NO-releasing capacity was investigated using NOA under 50 μM SNAP and 50 μM GSH (Fig. 1D). The NO generated by PLLA increased to 84.96 pM but ceased to generate afterward. On the other hand, both PM and PMZ showed initial maximum NO fluxes of 285.86 and 372.79 pM, respectively, and maintained average NO fluxes of 63.21, and 211.07 pM, respectively. Sustained NO generation also observed in PM, but the highest and most sustained NO concentration was found in the PMZ, likely due to NO-generating ability of metal oxides such as MH and ZO, with ZO showing the highest generation [24]. In addition, ZA included in PMZ generates more potent NO through surface-modification with ALA. As shown in Fig. 1D (b) and Fig. S3, the long-term NO generated by the functional microparticles was visualized

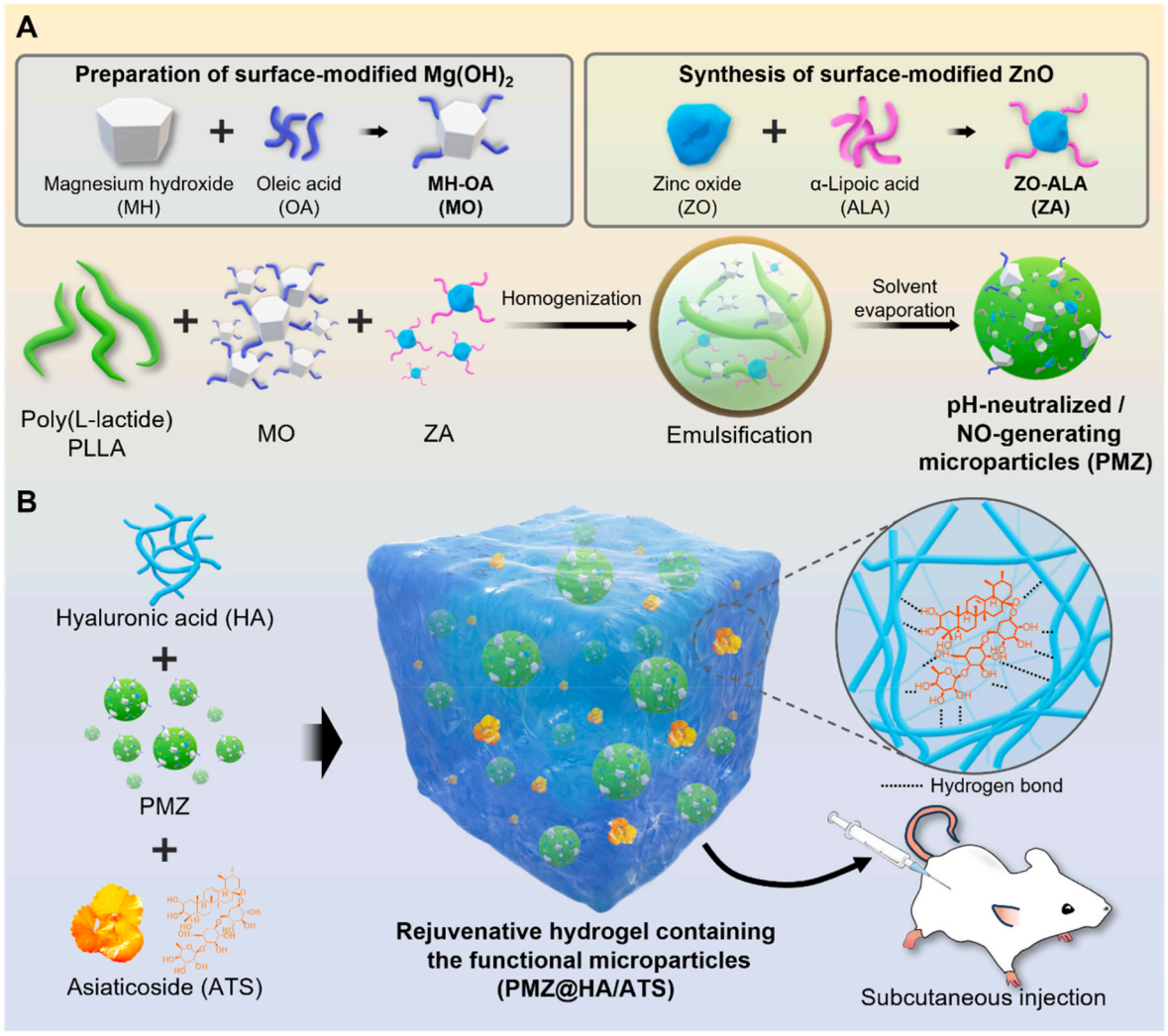

Scheme 1. Schematic illustration of the rejuvenative hydrogels containing functional microparticles. (A) Surface-modification of MH and ZO and fabrication of the pH neutralized and NO-generating microparticles. (B) Preparation of the rejuvenative hydrogels containing functional microparticles.

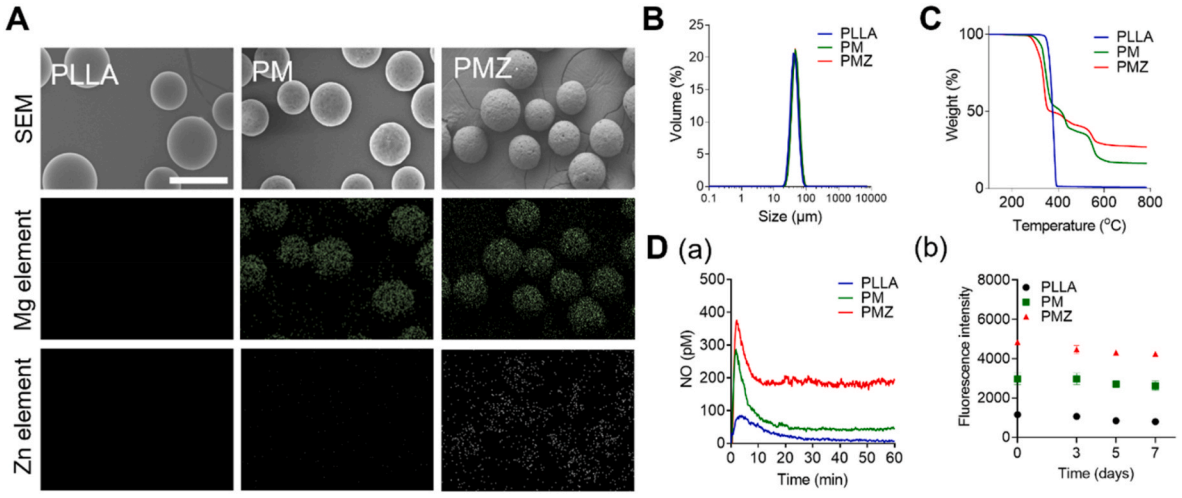

Fig. 1. Characterization of pH neutralized and NO-generating microparticles. (A) SEM and EDS mapping images (scale bar: 50 μm). (B) Size distribution. (C) TGA thermograms. (D) Real-time monitoring of NO generation flux using NOA (a) and quantitative fluorescence intensity was assessed using DAF-FM after immersion for 7 days (b) at 37 °C in PBS solution in the presence of NO donor.

(a) and quantified (b) by NO-sensitive fluorescent dye (DAF-FM). Fluorescence intensity was more robust in the PMZ, indicating higher NO production capacity. There was no notable variance in NO generation between 0 and 7 days across all groups.

3.2. Characterization of the rejuvenative hydrogels containing functional microparticles

Each PLLA, PM, and PMZ was mixed in an HA-based hydrogel to improve stability with a controlled release in the skin (PLLA@HA, PM@HA, and PMZ@HA, respectively). Additionally, the PMZ@HA included ATS (PMZ@HA/ATS) can effectively stimulate collagen production, antioxidant activity, and angiogenesis. Fig. 2 shows the characterization of the rejuvenative hydrogel containing the functional microparticles (PLLA@HA, PM@HA, PMZ@HA, and PMZ@HA/ATS). Fig. 2A displays SEM images of the rejuvenative hydrogel containing the functional microparticles. The spherical microparticles were revealed within the hydrogel in SEM images of PLLA@HA, PM@HA, PMZ@HA, and PMZ@HA/ATS, whereas only the porous structure of the hydrogel was observed. PMZ@HA/ATS had fewer pores than the other groups, with ATS occupying some pores, which might affect the hydrogel's mechanical properties. In addition, HA-based hydrogel contains numerous hydroxyl and carboxy groups, and ATS has 13 hydroxyl groups per molecule. Therefore, many hydrogen bonds can be formed between these two molecules, and the formed hydrogen bonds induce intermolecular entanglement and enhance viscosity [36,37].

The evaluation of rheological properties of rejuvanative hydrogels containing the functional microparticles, including the storage (G′) and the loss (G″) modulus, was conducted by adjusting the frequency (Fig. 2B). G′ and G" of all groups increased in proportion to frequency, with the highest increase observed in the PMZ@HA/ATS. Additionally, G′ was higher than G″ in all groups, and the difference between G′ and G″ became larger with increasing frequency. All groups' viscosity-to-elastic modulus (tan δ) of all groups maintained less than 1. Through these results, it was found that elastic behavior was dominant to viscous behavior in the rejuvenative hydrogels containing functional microparticles, the PMZ@HA/ATS has the most notable elasticity, and the presence of microparticles has no effect [38]. For clinician convenience, it is essential to keep the injection force constant when injecting hydrogel into the dermis [39]. In Fig. 2C, the mean injection force of HA, PLLA@HA, PM@HA, PMZ@HA, and PMZ@HA/ATS was 7.51 ± 0.29, 8.26 ± 0.03, 8.10 ± 0.24, 8.22 ± 0.18, and 9.64 ± 0.27 N, respectively. It slightly increased due to the presence of the functional microparticles and ATS, but it did not affect the maintenance the injection force. The

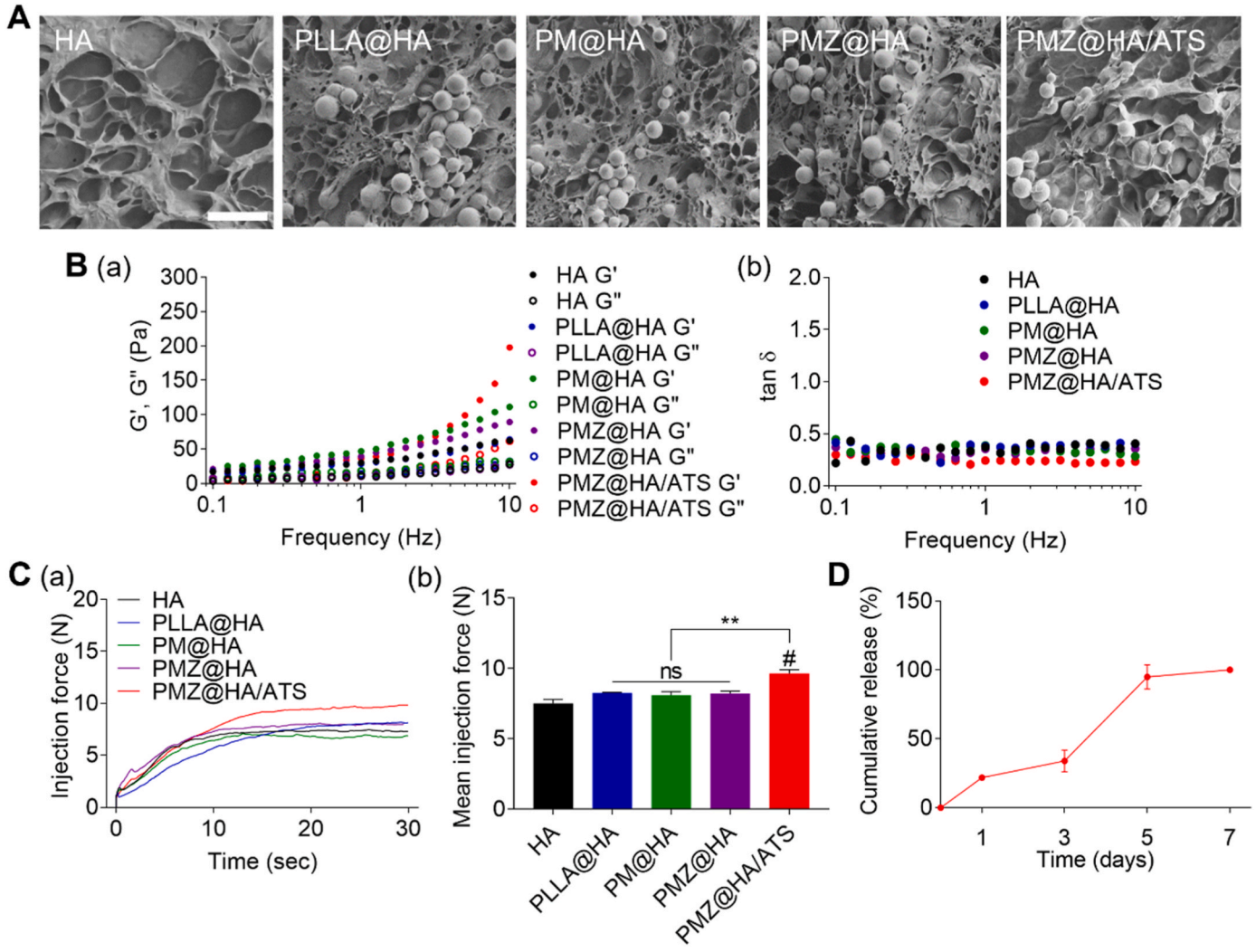

Fig. 2. Characterization of the rejuvenative hydrogels containing functional microparticles. (A) SEM images for NO-generating microparticles in hydrogel (scale bar: 200 μm). (B) Rheological properties; storage modulus (G′) and loss modulus (G″) (a) and Tan δ (b) under different frequencies. (C) Injection force (a) and mean injection force (b). (D) Cumulative release behavior of ATS from hydrogel in PBS solution at 37 °C. $^{**}p < 0.01$ and $^{\#}p < 0.0001$ indicate statistically significant differences, respectively.

release profile of ATS from PMZ@HA/ATS was measured for 4 weeks at 37 °C (Fig. 2D). The ATS was almost wholly released in 7 days with an initial boosting.

3.3. Biocompatibility and ROS scavenging capacity of rejuvenative hydrogels containing functional microparticles

The biocompatibility of the rejuvenative hydrogels containing functional microparticles was investigated using Live/Dead staining and CCK-8 assay (Fig. 3A and B). There was no significant morphological difference in Live/Dead fluorescent images of live cells in all groups, and the highest number of cells was observed in the PMZ@HA/ATS. Dead cells were rarely observed in all groups. The cell viability increased in the PMZ@HA and PMZ@HA/ATS for 5 days, compared to the HA, PLLA/HA, and PM/HA. Superior biocompatibility of the rejuvenative hydrogels containing functional microparticles was demonstrated through non-cytotoxicity and increased cell proliferation to hDFs. In addition, the inflammatory response has been contemplated as a crucial challenge in the progress of effective biomaterials. HA is a natural polymer synthesized in the human body and has high biocompatibility. However, as mentioned above, the surrounding tissue is acidified by lactic acid, a by-product of PLLA, which leads to inflammation and skin necrosis. Thus, the expression of inflammatory cytokines (IL-8, IL-6, IL-1β, and COX-2) was assessed by treating the degradation products of PLLA microparticles in hDFs (Fig. S4). As a result, the expression of inflammatory-related genes increased in PLLA compared to the control. However, the expression of inflammatory-related genes was reduced by the PM and PMZ because ZA and especially MO neutralized acidic by-products.

Abnormal accumulation of intracellular reactive oxygen species (ROS) can cause tissue damage through oxidative stress and cellular damage. Additionally, since ROS reacts with the generated NO to produce nitrate, a toxic substance, the ROS scavenging properties of NO-generating biomaterials is essential [40]. The free radical removal ability of the rejuvenative hydrogels containing functional microparticles was explored using DPPH, including free radicals (Fig. 3C). The proportion of DPPH activities decreased to 98 %, 87 %, 72 %, and 61 % over HA, respectively. The intracellular ROS in hDFs was visualized using DCF-DA as a ROS-specific fluorogenic marker (Fig. 3D). The most robust green fluorescence was observed in PLLA@HA. In contrast, negligible green fluorescence was shown in the other groups. The appearance of these results is related to pH neutralization effect and ROS

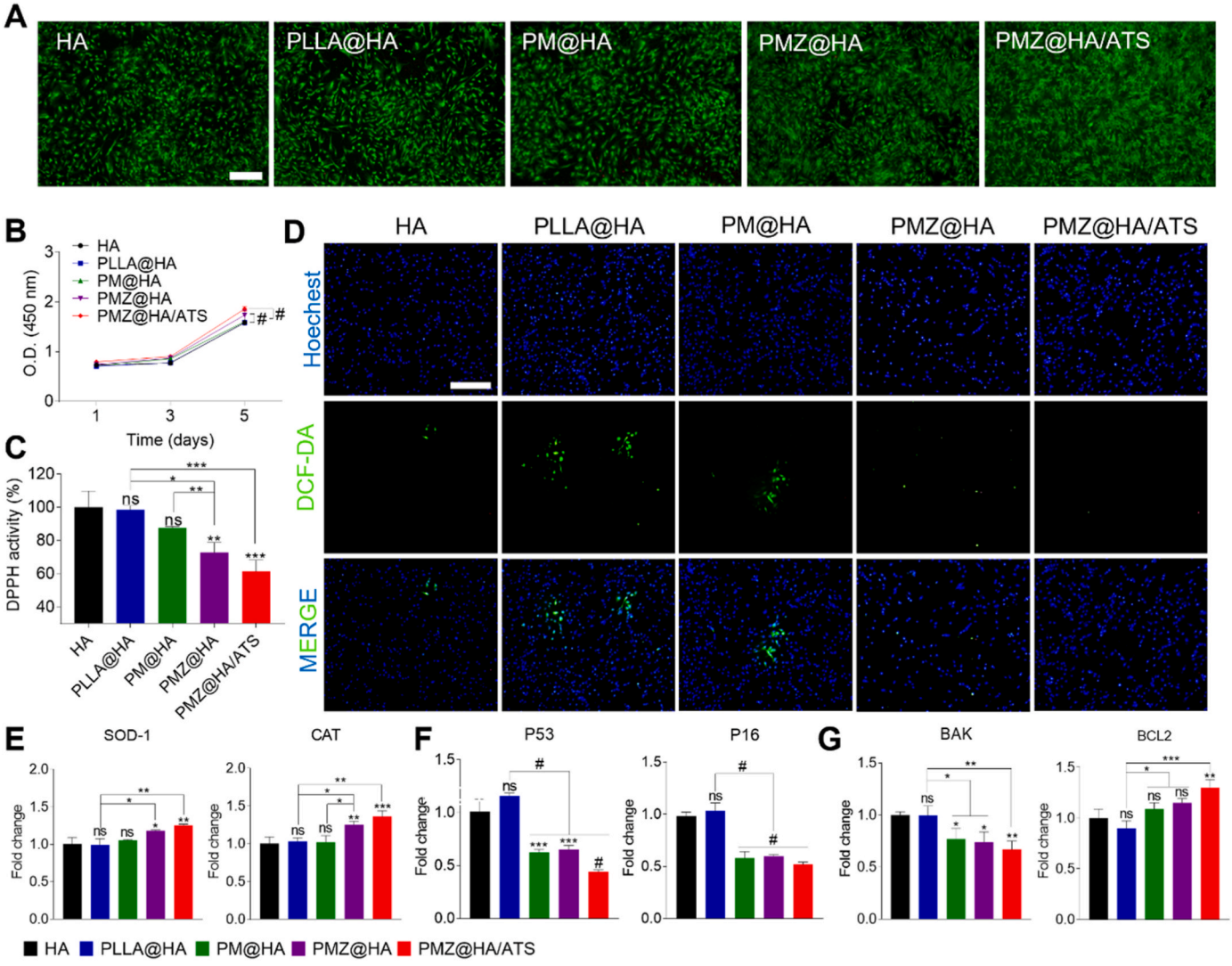

Fig. 3. *In vitro* evaluation of biocompatibility and ROS scavenging effects in hDFs to rejuvenative hydrogels containing functional microparticles. (A) Live-Dead assay images (scale bar: 500 μm) and (B) cell proliferation at 1, 3, and 5 days. (C) DPPH radical scavenging activity and (D) DCF-DA fluorescence images (scale bar: 500 μm). (E) mRNA expression level of ROS-related (SOD-1 and CAT), (F) senescence-related (P53 and P16), and (G) apoptosis-related (BAK and BCL2) genes. $^{*}p < 0.05$, $^{**}p < 0.01$, $^{***}p < 0.001$, and $^{\#}p < 0.0001$ indicate statistically significant differences, respectively.

scavenging ability of inorganic particles such as MH and ZO, but may be influenced by the released Zn ions. It has been known that superoxide and H_2O_2 can be scavenged by SOD1 and CAT, respectively [41,42]. The SOD1 typically depends on zinc and copper ions and prevents the transmutation of NO into nitrate [41,43]. As the concentration of zinc ions increases intracellularly, it accelerates the transformation of peroxide radical anions into H_2O_2. Sequentially, H_2O_2 is converted to H_2O by CAT and removed [44,45]. This enhanced process of ROS scavenging was evident in the upregulation of ROS scavenging-related genes (SOD1 and CAT) in the zinc-including groups (Fig. 3E). In particular, the expression of related genes was investigated since excessive ROS production and weakened antioxidant mechanisms induce cell senescence and apoptosis in skin tissues [39].

In Fig. 3F, the expression levels of cellular senescence-related genes (P53 and P16) significantly decreased in the PM@HA, PMZ@HA, and PMZ@HA/ATS, compared to the HA and PLLA@HA. Fig. 3G displays the expression levels of apoptotic-related genes. The expression of BAK as a proapoptotic-related gene was downregulated in the PM@HA, PMZ@HA, and PMZ@HA/ATS. In contrast, the expression of BCL-2 as an antiapoptotic-related gene was the highest in the PMZ@HA/ATS. These results implied that the rejuvenative hydrogels containing functional microparticles possess excellent anti-inflammatory and ROS-scavenging properties as a dermal injecting hydrogel.

3.4. *Collagen biosynthesis by rejuvenative hydrogels containing functional microparticles*

Collagen provides structure and support to tissues, especially in the skin. Therefore, as the injected hydrogel is decomposed, collagen production is essential for maintaining function and restoring the skin volume [18]. In Fig. 4, collagen biosynthesis by the rejuvenative hydrogels containing functional microparticles was investigated. The expression levels of collagen biosynthesis-related (COL1A1, COL3A1, and TGF-β1), and elastin formatting-related (Elastin) genes were upregulated in PMZ@HA and PMZ@HA/ATS. The mRNA expression levels were most highly up-regulated in PMZ@HA/ATS, and the expression levels of TGF-β1 and Elastin slightly increased in PM@HA. The TGF-β is well-recognized as the regulator of collagen production and wound repair systems modulated by ATS [2]. The expression and activation of the TGF-β1 were also regulated by NO and related redox species [46]. Elastin rebounds stretched or compressed skin and, together with collagen, keeps the skin's flexibility and resilience. The expression levels of MMP1 progressively decreased in PM@HA, PMZ@HA, and PMZ@HA/ATS. Since the skin mainly comprises collagen type 1, the

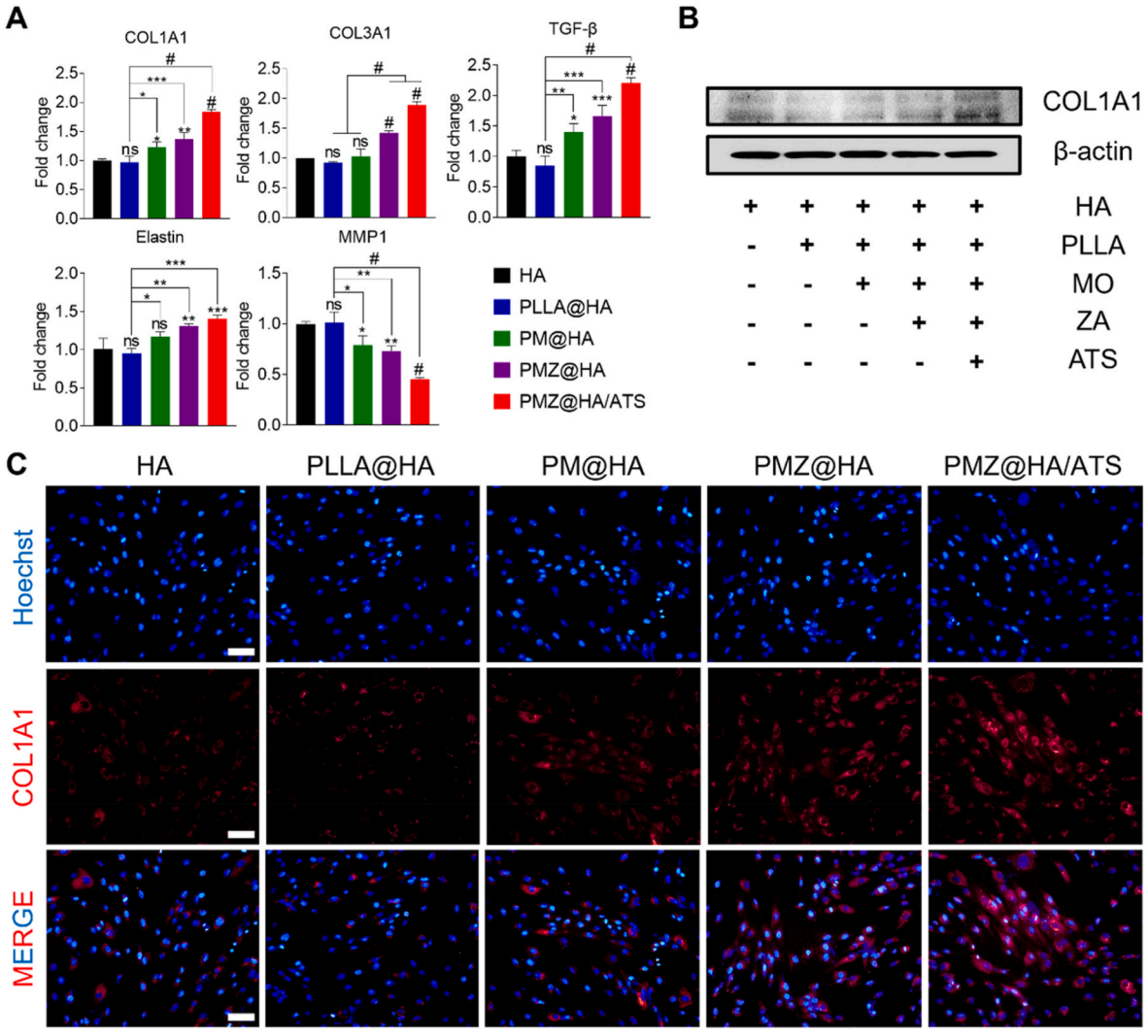

Fig. 4. *In vitro* collagen biosynthesized effect of rejuvenative hydrogel containing the functional microparticles in hDFs. (A) mRNA expression levels of collagen biosynthesis-related (COL1A1, COL3A1, TGF-β, and Elastin) and collagen degradation-related (MMP1) genes. (B) Western blot analysis and (C) representative immunocytochemistry (ICC) staining images for collagen biosynthesis-related (COL1A1) protein expression (scale bar: 100 μm). $^{*}p < 0.05$, $^{**}p < 0.01$, $^{***}p < 0.001$, and $^{\#}p < 0.0001$ indicate statistically significant differences, respectively.

protein marker related to collagen biosynthesis (COL1A1) was intensively evaluated. The expression of COL1A1 was upregulated in the PMZ@HA/ATS (Fig. 4B). Representative visualized fluorescent images of the expression of COL1A1 were also the highest in PMZ@HA/ATS (Fig. 4C). Biosynthesis and degradation of collagen were regulated by the rejuvenating hydrogels containing the functional microparticles and could be effective for the rejuvenation and regeneration of skin tissues, just as NO and ATS promoted collagen deposition and wound healing in many studies [23,47].

3.5. Angiogenic efficiency of the rejuvenative hydrogel containing functional microparticles

Maintaining intact blood vessels in the skin is essential for promoting skin regeneration [48], so the angiogenic effect of the rejuvenative hydrogels containing functional microparticles was verified in Fig. 5. The proliferation and migration of HUVECs were analyzed in the presence of a NO donor (Figs. S6 and S7). The cell proliferation and migration ability increased in groups capable of generating NO, and the most significant increase occurred in PMZ@HA/ATS. A tube-formation assay verified the vessel-generating capacity of PMZ@HA/ATS (Fig. 5A). The total tube length and the number of branching points in representative fluorescent images and associative quantitative gradually rose in PM@HA, PMZ@HA, and PMZ@HA/ATS due to the synergistic effects of NO and ATS promoting VEGF secretion [49,50]. To demonstrate the synergistic effects of NO and ATS, mRNA expression of NO-related (HIF-1α), pro-angiogenic markers (ANGPT-1 and VEGF) and endothelial activity-related (eNOS) was evaluated as shown in Fig. 5B, and expression levels of all genes were upregulated in PMZ@HA and PMZ@HA/ATS. The NO induces the hypoxia-response but inhibits HIF-1α degradation by prolyl hydroxylation reaction. Consecutively, HIF-1α triggered the induction of VEGF [51,52]. Although the expression level of HIF-1α did not indicate a difference between the PMZ@HA and PMZ@HA/ATS, the expression of ANGPT-1 and VEGF was higher in the PMZ@HA/ATS, supporting the promotion of VEGF expression by ATS. Due to the influence of such gene expression, genes related to endothelial cell activity was also the highest in PMZ@HA/ATS.

3.6. Volume retention ability and histological assessments

To demonstrate volume retention and skin regeneration, the remaining hydrogel and histological evaluation were performed at 4, 8, and 16 weeks after subcutaneous injection of the rejuvenative hydrogels containing functional microparticles into mice. To investigate the effects of the rejuvenative hydrogels containing functional microparticles in the tissue, H&E and MT were performed (Fig. 6C and D and Figs. S9 and S10). Compared to native group (N), no abnormal morphological changes were observed in the rejuvenative hydrogels containing functional microparticles, and several blood vessels and thickened collagen walls were more visually observed in the PMZ@HA and PMZ@HA/ATS. In addition, the expression of inflammatory factors was effectively suppressed by MO and ZA (Fig. S11).

Fig. 7A represents the mRNA genes expression after 16 weeks of injection. The expression levels of collagen biosynthesis-related genes (COL1A1, COL3A1, and Elastin) were gradually upregulated in PMZ@HA and PMZ@HA/ATS (Fig. 7A(a)). However, an abnormal overexpression of collagen may induce fibrosis. As fibrosis progresses, hyperplasia of smooth muscle cells is induced in tissues from the muscle layer to the fat layer [4]. SMA expression and the contractile ability are reduced by hyperplasia of smooth muscle cells [53]. In other words, decreased α-SMA expression could be associated with the development of fibrosis. Therefore, we investigated the gene expression of α-SMA (Fig. 7A(b)). Expression of α-SMA was downregulated in PLLA@HA,

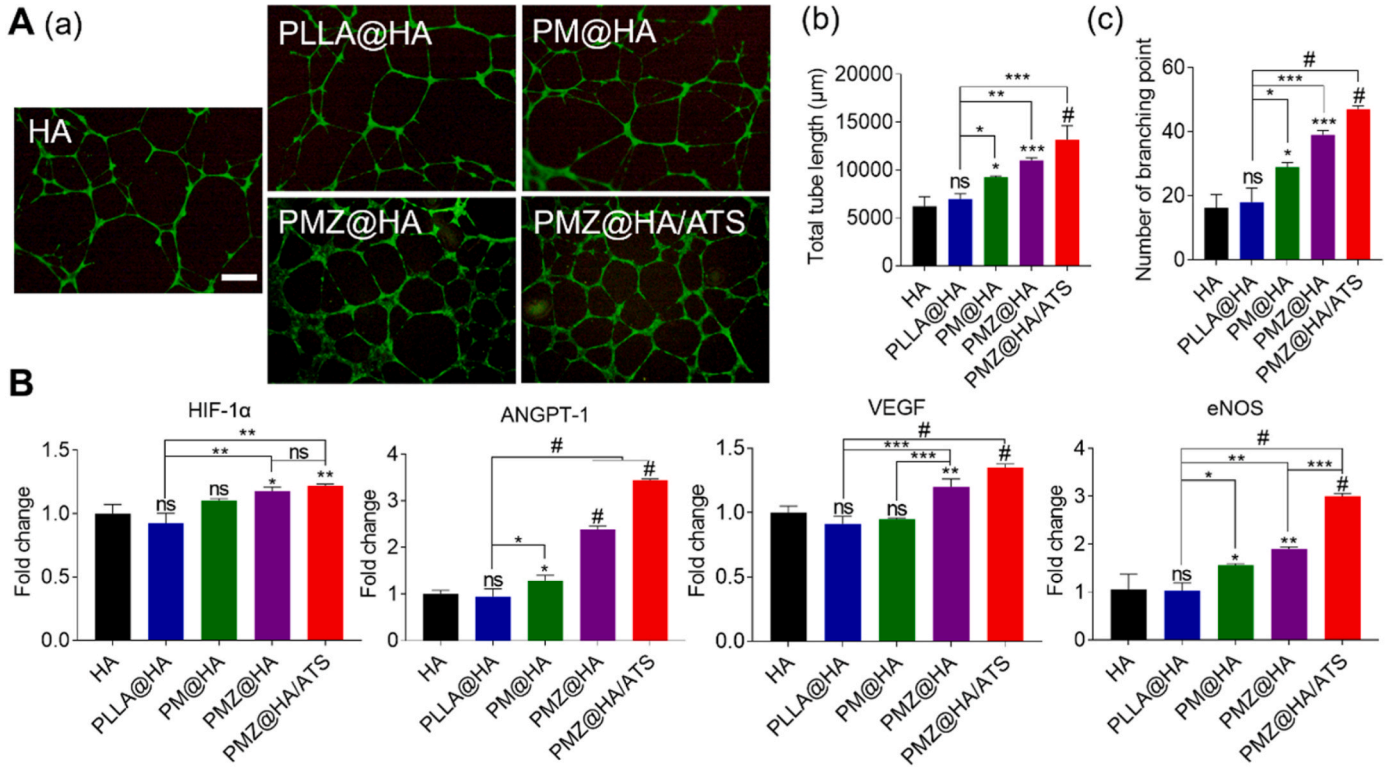

Fig. 5. Angiogenetic ability evaluation by NO generation of rejuvenative hydrogels containing functional microparticles using HUVECs. (A) Representative fluorescent images of stained with calcein AM (a), quantification of total tube length (b), and the number of branching points (c) of the tubule-forming assay (scale bar: 200 μm). (B) The mRNA expression levels of NO generation-related gene (HIF-1α) and angiogenesis-related genes (ANGPT-1, VEGF, and eNOS). $^{*}p < 0.05$, $^{**}p < 0.01$, $^{***}p < 0.001$, and $^{\#}p < 0.0001$ indicate statistically significant differences, respectively.

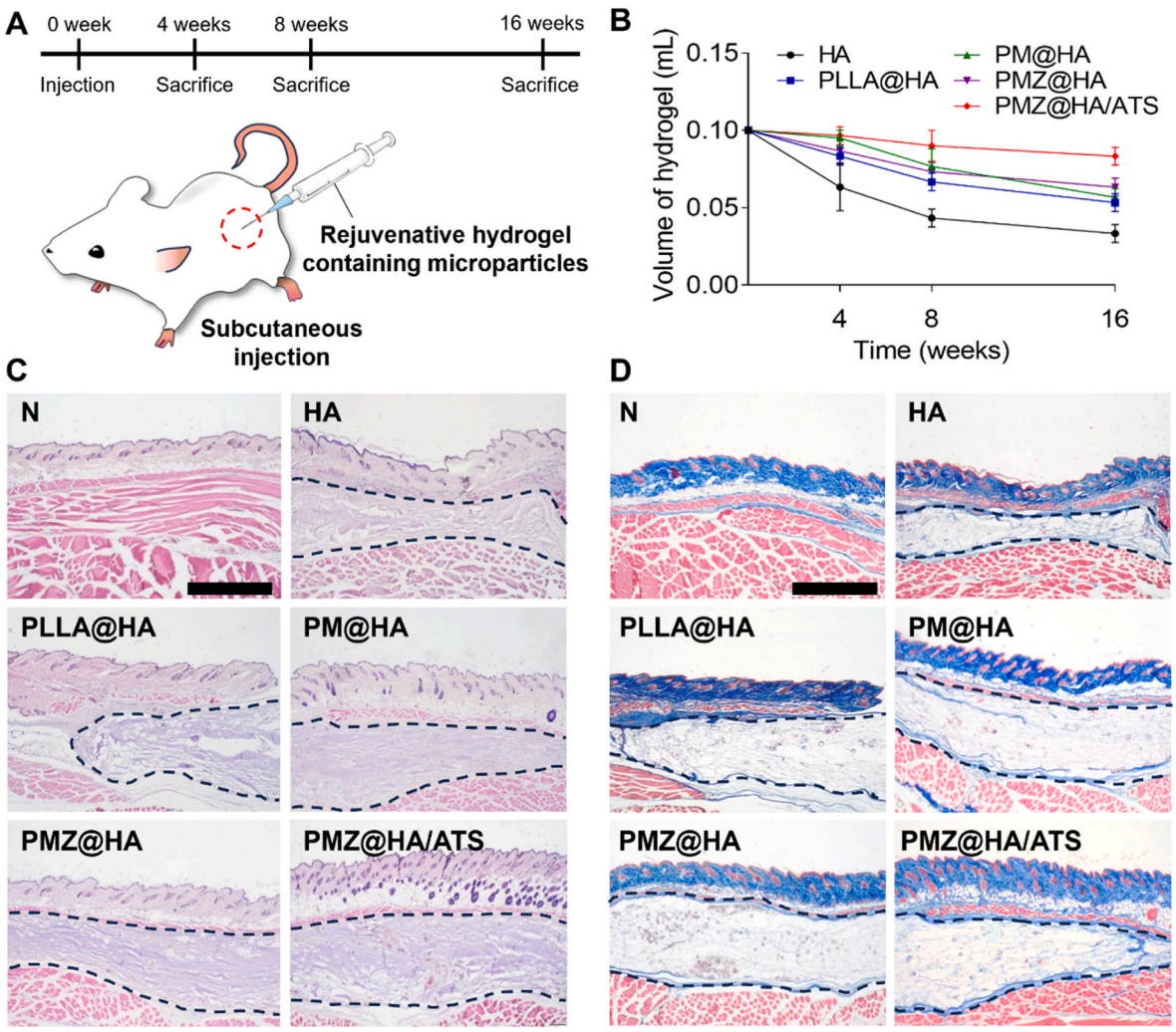

Fig. 6. Histological assessment after subcutaneous injection of rejuvenative hydrogels containing functional microparticles into mice. (A) Schematic illustrations of the *in vivo* experimental images. (B) Quantitative residual volumes of hydrogel at 4, 8, and 16 weeks. (C) Hematoxylin and Eosin (H&E) staining and (D) Masson's Trichrome (MT) staining images of the dermal tissues at 16 weeks (scale bar: 1 mm).

whereas other groups were similar to native. Although the expression of collagen biosynthesis-related genes increased significantly in PMZ@HA/ATS, the expression of α-SMA was maintained, proving that fibrosis was not induced. Expression of NO-related (HIF-1α) and angiogenesis-related genes (ANGPT1 and VEGF) were upregulated in PMZ@HA and PMZ@HA/ATS, similar to *in vitro* mRNA evaluation (Fig. 7A(c)). Fig. 7B displays the protein expression of COL1A1, being highest in PMZ@HA/ATS. In Fig. 7C, immunofluorescent (IF) staining was conducted to demonstrate the VCAM-1-mediated immune response in the blood vessels by the rejuvenative hydrogels containing functional microparticles. DAPI and CD31 were used as markers as nuclear and vascular endothelial cells, respectively. Expression of VCAM-1 in the PLLA@HA was observed with strong fluorescence, whereas gradually lower expression was found in the PM@HA, PMZ@HA, and PMZ@HA/ATS. VCAM-1 is inducible and predominantly expressed in endothelial cells and macrophage membranes. VCAM-1 expression activated by inflammatory cytokines results in the accumulation of VCAM-1 adhesion molecules in endothelium and membranes [54]. MO diminished the PLLA-induced inflammatory response in the PMZ@HA/ATS and consequently had a remarkable effect on maintaining healthy blood vessels with NO generation. Overall, the PMZ@HA/ATS can regenerate the skin through collagen biosynthesis and angiogenesis without causing fibrosis.

4. Conclusions

We successfully fabricated surface-modified inorganic particles, pH neutralized and NO-generating microparticles, and the rejuvenative hydrogels containing functional microparticles, a novel delivery system for rejuvenation and regeneration of skin tissue. The functional microparticles provided pH neutralized and NO generation effects and it was demonstrated in *in vitro* and *in vivo* that the rejuvenative hydrogels containing functional microparticles and ATS improved volume retention, ROS scavenging effects, collagen biosynthesis, anti-inflammation, and angiogenesis capabilities by synergistic effects. These regenerative hydrogels containing the functional microparticles hold significant promise in the field of wound healing, as they promote substantial skin regeneration without inducing fibrosis. Meanwhile, in the cosmetology, it seems to be able to draw attention by reduced wrinkles and maintained excellent volume. In summary, our injectable PMZ@HA/ATS with controlled release of bioactive molecules presented a cutting-edge technology for skin regeneration and facial rejuvenation. It believes that this advancement holds significant potential for enhancing the overall well-being and appearance of individuals seeking effective and non-invasive solutions for skin rejuvenation.

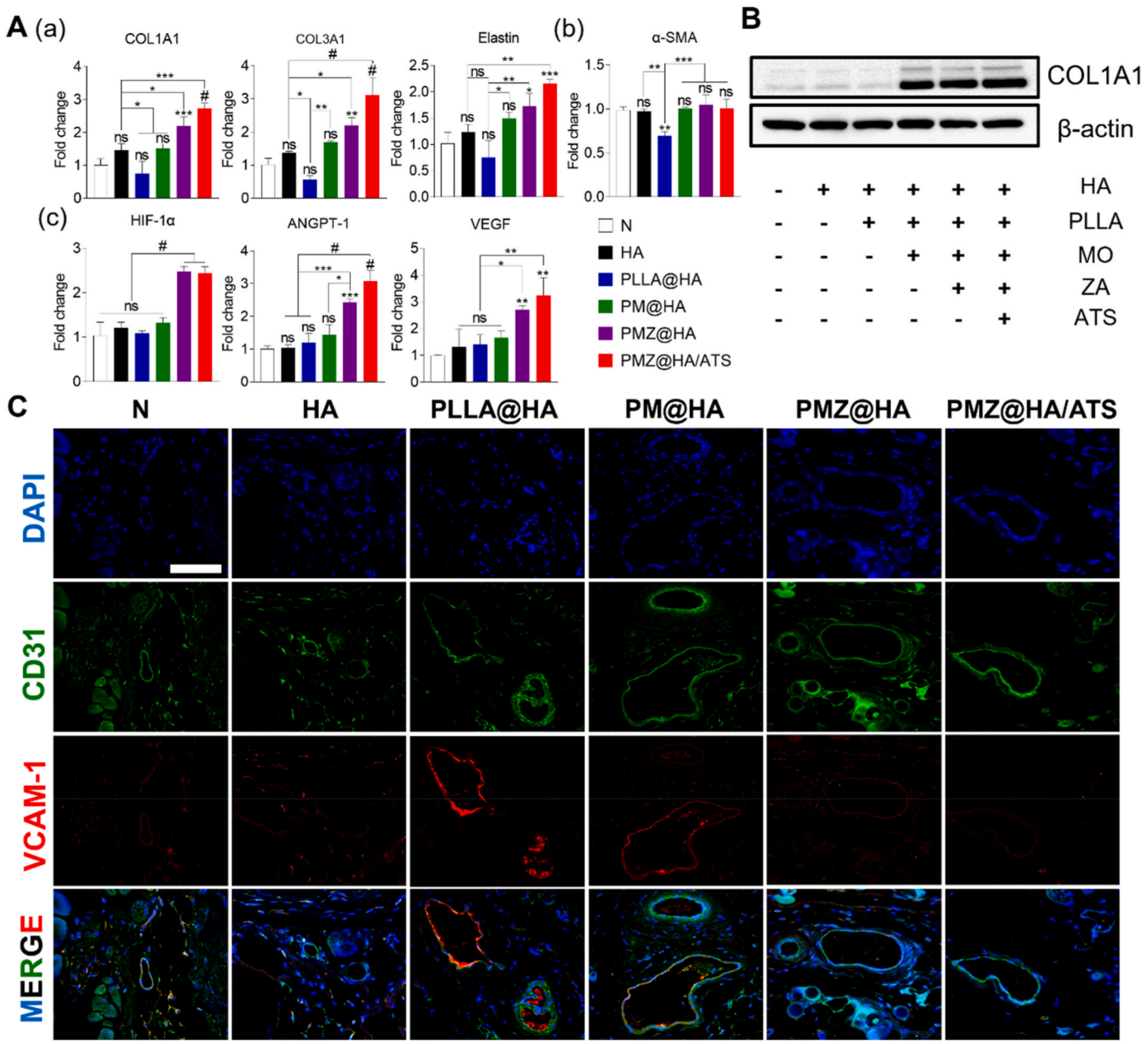

Fig. 7. Collagen biosynthesis and angiogenesis in dermal tissues at 16 weeks after subcutaneous injection of rejuvenative hydrogels containing functional microparticles into mice. (A) mRNA expression levels of collagen-related (COL1A1, COL3A1, and Elastin) (a), fibrosis-related (α-SMA) (b), and angiogenesis-related (HIF-1α, ANGPT-1 and VEGF) (c) genes. (B) Western blot analysis of collagen biosynthesis-related protein (COL1A1). (C) Immunohistochemistry staining (IHC) images of CD31 (green), VCAM-1 (red), and DAPI (blue) (scale bar: 100 μm). $^{*}p < 0.05$, $^{**}p < 0.01$, $^{***}p < 0.001$, and $^{\#}p < 0.0001$ indicate statistically significant differences, respectively.

CRediT authorship contribution statement

Semi Lee: Conceptualization, Validation, Writing - original draft, Writing - review & editing. **Seung-Woon Baek:** Conceptualization, Validation, Writing - original draft. **Da-Seul Kim:** Data curation, Investigation, Visualization. **So-Yeon Park:** Data curation, Investigation. **Jun Hyuk Kim:** Data curation, Investigation, Validation. **Ji-Won Jung:** Data curation, Investigation, Validation. **Jun-Kyu Lee:** Investigation, Validation. **Gi-Min Park:** Data curation, Investigation. **Chun Gwon Park:** Writing - review & editing. **Dong Keun Han:** Funding acquisition, Supervision, Writing - review & editing.

Declaration of competing interest

The authors declare that they have no known competing financial interests or personal relationships that could have appeared to influence the work reported in this paper.

Data availability

Data will be made available on request.

Acknowledgments

This work was supported by the Korea Medical Device Development Grant funded by the Korea Government (the Ministry of Science and ICT,

the Ministry of Trade, Industry and Energy, the Ministry of Health & Welfare, the Ministry of Food and Drug Safety) (Project Number: 1711195494, RS-2020-KD000005 and Project Number: 1711196421, RS-2023-00255811) and the Korean Fund for Regenerative Medicine (KFRM) Grant funded by the Korea Government (the Ministry of Science and ICT, the Ministry of Health & Welfare) (23A0206L1).

Appendix A. Supplementary data

Supplementary data to this article can be found online at https://doi.org/10.1016/j.mtbio.2023.100890.

References

[1] W.Y. Jeong, M. Kwon, H.E. Choi, K.S. Kim, Recent advances in transdermal drug delivery systems: a review, Biomater. Res. 25 (1) (2021) 24, https://doi.org/10.1186/s40824-021-00226-6.

[2] S. Liu, Y. Zhao, M. Li, L. Nie, Q. Wei, O.V. Okoro, H. Jafari, S. Wang, J. Deng, J. Chen, A. Shavandi, L. Fan, Bioactive wound dressing based on decellularized tendon and GelMA with incorporation of PDA-loaded asiaticoside nanoparticles for scarless wound healing, Chem. Eng. J. 466 (2023), 143016, https://doi.org/10.1016/j.cej.2023.143016.

[3] S.S. Johl, R.A. Burgett, Dermal filler agents: a practical review, Curr. Opin. Ophthalmol. 17 (5) (2006) 471–479, https://doi.org/10.1097/01.icu.0000243021.20499.4b.

[4] R. Curciarello, G.H. Docena, T.T. MacDonald, The role of cytokines in the fibrotic responses in crohn's disease, Front. Med. 4 (2017) 126, https://doi.org/10.3389/fmed.2017.00126.

[5] X. Gao, S. Ma, X. Xing, J. Yang, X. Xu, C. Liang, Y. Yu, L. Liu, L. Liao, W. Tian, Microvessels derived from hiPSCs are a novel source for angiogenesis and tissue regeneration, J. Tissue Eng. 13 (2022), 20417314221143240, https://doi.org/10.1177/20417314221143240.

[6] N.I. Md Fadilah, M.S. Mohd Abdul Kader Jailani, M.A.I. Badrul Hisham, N. Sunthar Raj, S.A. Shamsuddin, M.H. Ng, M.B. Fauzi, M. Maarof, Cell secretomes for wound healing and tissue regeneration: next generation acellular based tissue engineered products, J. Tissue Eng. 13 (2022), 20417314221114273, https://doi.org/10.1177/20417314221114273.

[7] Y. Dong, M. Cui, J. Qu, X. Wang, S.H. Kwon, J. Barrera, N. Elvassore, G.C. Gurtner, Conformable hyaluronic acid hydrogel delivers adipose-derived stem cells and promotes regeneration of burn injury, Acta Biomater. 108 (2020) 56–66, https://doi.org/10.1016/j.actbio.2020.03.040.

[8] B.M. Hong, S.A. Park, W.H. Park, Effect of photoinitiator on chain degradation of hyaluronic acid, Biomater. Res. 23 (2019) 21, https://doi.org/10.1186/s40824-019-0170-1.

[9] J. Zeng, X. Chen, J. Zhang, Y. Qin, K. Zhang, X. Li, H. Cui, Stem cell spheroids production for wound healing with a reversible porous hydrogel, Mate Today Adv 15 (2022), 100269, https://doi.org/10.1016/j.mtadv.2022.100269.

[10] S. You, Y. Xiang, X. Qi, R. Mao, E. Cai, Y. Lan, H. Lu, J. Shen, H. Deng, Harnessing a biopolymer hydrogel reinforced by copper/tannic acid nanosheets for treating bacteria-infected diabetic wounds, Mater Today Adv 15 (2022), 100271, https://doi.org/10.1016/j.mtadv.2022.100271.

[11] N. Sällström, A. Capel, M.P. Lewis, D.S. Engstrøm, S. Martin, 3D-printable zwitterionic nano-composite hydrogel system for biomedical applications, J. Tissue Eng. 11 (2020), 2041731420967294, https://doi.org/10.1177/2041731420967294.

[12] A. Abu-Hakmeh, A. Kung, B.R. Mintz, S. Kamal, J.A. Cooper, X.L. Lu, L.Q. Wan, Sequential gelation of tyramine-substituted hyaluronic acid hydrogels enhances mechanical integrity and cell viability, Med. Biol. Eng. Comput. 54 (12) (2016) 1893–1902, https://doi.org/10.1007/s11517-016-1474-0.

[13] S.-W. Shin, Y.-D. Jang, K.-W. Ko, E.Y. Kang, J.-H. Han, T.M. Bedair, I.-H. Kim, T.-I. Son, W. Park, D.K. Han, PCL microspheres containing magnesium hydroxide for dermal filler with enhanced physicochemical and biological performances, J. Ind. Eng. Chem. 80 (2019) 854–861, https://doi.org/10.1016/j.jiec.2019.07.043.

[14] T.R. Kwon, S.W. Han, I.K. Yeo, J.H. Kim, J.M. Kim, J.Y. Hong, B.C. Lee, S.E. Lee, H. S. Moon, H.J. Kwon, B.J. Kim, Biostimulatory effects of polydioxanone, poly-d, l lactic acid, and polycaprolactone fillers in mouse model, J. Cosmet. Dermatol. 18 (4) (2019) 1002–1008, https://doi.org/10.1111/jocd.12950.

[15] Y. Zhang, H. Liang, Q. Luo, J. Chen, N. Zhao, W. Gao, Y. Pu, B. He, J. Xie, In vivo inducing collagen regeneration of biodegradable polymer microspheres, Regen Biomater 8 (5) (2021), https://doi.org/10.1093/rb/rbab042 rbab042.

[16] S.W. Baek, D.S. Kim, D.H. Song, H.B. Kim, S. Lee, J.H. Kim, J.K. Lee, Y.J. Hong, C. G. Park, D.K. Han, Reduced restenosis and enhanced re-endothelialization of functional biodegradable vascular scaffolds by everolimus and magnesium hydroxide, Biomater. Res. 26 (1) (2022) 86, https://doi.org/10.1186/s40824-022-00334-x.

[17] S.W. Baek, D.H. Song, H.I. Lee, D.S. Kim, Y. Heo, J.H. Kim, C.G. Park, D.K. Han, Poly(L-Lactic acid) composite with surface-modified magnesium hydroxide nanoparticles by biodegradable oligomer for augmented mechanical and biological properties, Materials 14 (19) (2021) 5869, https://doi.org/10.3390/ma14195869.

[18] Y. Heo, S.W. Shin, D.S. Kim, S. Lee, S.Y. Park, S.W. Baek, J.K. Lee, J.H. Kim, D. K. Han, Bioactive PCL microspheres with enhanced biocompatibility and collagen production for functional hyaluronic acid dermal fillers, Biomater. Sci. 10 (4) (2022) 947–959, https://doi.org/10.1039/d1bm01846a.

[19] T.M. Bedair, C.K. Lee, D.S. Kim, S.W. Baek, H.M. Bedair, H.P. Joshi, U.Y. Choi, K. H. Park, W. Park, I. Han, D.K. Han, Magnesium hydroxide-incorporated PLGA composite attenuates inflammation and promotes BMP2-induced bone formation in spinal fusion, J. Tissue Eng. 11 (2020), 2041731420967591, https://doi.org/10.1177/2041731420967591.

[20] D.S. Kim, J.K. Lee, J.W. Jung, S.W. Baek, J.H. Kim, Y. Heo, T.H. Kim, D.K. Han, Promotion of bone regeneration using bioinspired PLGA/MH/ECM scaffold combined with bioactive PDRN, Materials 14 (15) (2021) 4149, https://doi.org/10.3390/ma14154149.

[21] S.W. Baek, D.S. Kim, D.H. Song, S. Lee, J.K. Lee, S.Y. Park, J.H. Kim, T.H. Kim, C. G. Park, D.K. Han, PLLA composites combined with delivery system of bioactive agents for anti-inflammation and Re-endothelialization, Pharmaceutics 14 (12) (2022) 2661, https://doi.org/10.3390/pharmaceutics14122661.

[22] J.K. Lee, D.S. Kim, S.Y. Park, S.W. Baek, J.W. Jung, T.H. Kim, D.K. Han, Nitric oxide-releasing bioinspired scaffold for exquisite regeneration of osteoporotic bone via regulation of homeostasis, Adv. Sci. 10 (6) (2023), e2205336, https://doi.org/10.1002/advs.202205336.

[23] G. Liu, L. Wang, Y. He, L. Wang, Z. Deng, J. Liu, D. Peng, T. Ding, L. Lu, Y. Ding, J. Zhang, P. Liu, K. Cai, Polydopamine nanosheets doped injectable hydrogel with nitric oxide release and photothermal effects for bacterial ablation and wound healing, Adv. Healthcare Mater. 10 (23) (2021), e2101476, https://doi.org/10.1002/adhm.202101476.

[24] T. Yang, A.S. Fruergaard, A.K. Winther, A.N. Zelikin, R. Chandrawati, Zinc oxide particles catalytically generate nitric oxide from endogenous and exogenous prodrugs, Small 16 (27) (2020), e1906744, https://doi.org/10.1002/smll.201906744.

[25] S.-W. Baek, D.-S. Kim, J.-K. Lee, J.H. Kim, S. Lee, J.M. Park, S.-Y. Park, D.H. Song, C.G. Park, D.K. Han, Continuous NO dual-generation by ZnO nanoparticle conjugated with α-lipoic acid for functional biodegradable vascular stent, Chem. Eng. J. 470 (2023), 144174, https://doi.org/10.1016/j.cej.2023.144174.

[26] X. Lv, Y. Xu, X. Ruan, D. Yang, J. Shao, Y. Hu, W. Wang, Y. Cai, Y. Tu, X. Dong, An injectable and biodegradable hydrogel incorporated with photoregulated NO generators to heal MRSA-infected wounds, Acta Biomater. 146 (2022) 107–118, https://doi.org/10.1016/j.actbio.2022.05.006.

[27] Y. Cai, X. Xu, M. Wu, J. Liu, J. Feng, J. Zhang, Multifunctional zwitterionic microneedle dressings for accelerated healing of chronic infected wounds in diabetic rat models, Biomater. Sci. 11 (8) (2023) 2750–2758, https://doi.org/10.1039/d2bm02101c.

[28] S.W. Baek, J.H. Kim, D.H. Song, D.S. Kim, C.G. Park, D.K. Han, Enhanced mechanical properties and anti-inflammation of poly(L-lactic acid) by stereocomplexes of PLLA/PDLA and surface-modified magnesium hydroxide nanoparticles, Polymers 14 (18) (2022) 3790, https://doi.org/10.3390/polym14183790.

[29] H. Kamiya, M. Iijima, Surface modification and characterization for dispersion stability of inorganic nanometer-scaled particles in liquid media, Sci. Technol. Adv. Mater. 11 (4) (2010), 044304, https://doi.org/10.1088/1468-6996/11/4/044304.

[30] C. Shuai, L. Yu, P. Feng, S. Peng, H. Pan, X. Bai, Construction of a stereocomplex between poly(D-lactide) grafted hydroxyapatite and poly(L-lactide): toward a bioactive composite scaffold with enhanced interfacial bonding, J. Mater. Chem. B 10 (2) (2022) 214–223, https://doi.org/10.1039/d1tb02111g.

[31] D.S. Kim, J.H. Kim, S.W. Baek, J.K. Lee, S.Y. Park, B. Choi, T.H. Kim, K. Min, D. K. Han, Controlled vitamin D delivery with injectable hyaluronic acid-based hydrogel for restoration of tendinopathy, J. Tissue Eng. 13 (2022), 20417314221122089, https://doi.org/10.1177/20417314221122089.

[32] J. Ibarra, J. Melendres, M. Almada, M.G. Burboa, P. Taboada, J. Juárez, M. A. Valdez, Synthesis and characterization of magnetite/PLGA/chitosan nanoparticles, Mater. Res. Express 2 (9) (2015), 095010, https://doi.org/10.1088/2053-1591/2/9/095010.

[33] G.D. Zhao, R. Sun, S.L. Ni, Q. Xia, Development and characterisation of a novel chitosan-coated antioxidant liposome containing both coenzyme Q10 and alpha-lipoic acid, J. Microencapsul. 32 (2) (2015) 157–165, https://doi.org/10.3109/02652048.2014.973072.

[34] D. Sacks, B. Baxter, B.C.V. Campbell, J.S. Carpenter, C. Cognard, D. Dippel, M. Eesa, U. Fischer, K. Hausegger, J.A. Hirsch, M. Shazam Hussain, O. Jansen, M. V. Jayaraman, A.A. Khalessi, B.W. Kluck, S. Lavine, P.M. Meyers, S. Ramee, D. A. Rüfenacht, C.M. Schirmer, D. Vorwerk, Multisociety consensus quality improvement revised consensus statement for endovascular therapy of acute ischemic stroke, Int. J. Stroke 13 (6) (2018) 612–632, https://doi.org/10.1177/1747493018778713.

[35] D.H. Kim, D.S. Kim, H.J. Ha, J.W. Jung, S.W. Baek, S.H. Baek, T.H. Kim, J.C. Lee, E. Hwang, D.K. Han, Fat graft with allograft adipose matrix and magnesium hydroxide-incorporated PLGA microspheres for effective soft tissue reconstruction, Tissue Eng Regen Med 19 (3) (2022) 553–563, https://doi.org/10.1007/s13770-021-00426-0.

[36] S.N. Kirmic Cosgun, D. Ceylan Tuncaboylu, Cyclodextrin-linked PVP/PEG supramolecular hydrogels, Carbohydr. Polym. 269 (2021), 118278, https://doi.org/10.1016/j.carbpol.2021.118278.

[37] X. Ma, T. Xu, W. Chen, H. Qin, B. Chi, Z. Ye, Injectable hydrogels based on the hyaluronic acid and poly (γ-glutamic acid) for controlled protein delivery, Carbohydr. Polym. 179 (2018) 100–109, https://doi.org/10.1016/j.carbpol.2017.09.071.

[38] N. Salimiyan, M. Gholami, R. Sedghi, Preparation of degradable, biocompatible, conductive and multifunctional chitosan/thiol-functionalized graphene

nanocomposite hydrogel via click chemistry for human motion sensing, Chem. Eng. J. 471 (2023), 144648, https://doi.org/10.1016/j.cej.2023.144648.
[39] D.G. You, J.Y. An, W. Um, J.M. Jung, B.H. Oh, V.Q. Nguyen, J. Jeon, J. Lee, D. G. Jo, Y.W. Cho, J.H. Park, Stem cell-derived extracellular vesicle-bearing dermal filler ameliorates the dermis microenvironment by supporting CD301b-expressing macrophages, ACS Nano 16 (1) (2022) 251–260, https://doi.org/10.1021/acsnano.1c06096.
[40] B. Skibska, A. Goraca, The protective effect of lipoic acid on selected cardiovascular diseases caused by age-related oxidative stress, Oxid. Med. Cell. Longev. 2015 (2015), 313021, https://doi.org/10.1155/2015/313021.
[41] A.M.T. Gusti, S.Y. Qusti, E.M. Alshammari, E.A. Toraih, M.S. Fawzy, Antioxidants-related superoxide dismutase (SOD), catalase (CAT), glutathione peroxidase (gpx), glutathione-S-transferase (gst), and nitric oxide synthase (NOS) gene variants analysis in an obese population: a preliminary case-control study, Antioxidants 10 (4) (2021) 595, https://doi.org/10.3390/antiox10040595.
[42] H. Ding, S. George, X.I. Leng, M. Ihnat, J.X. Ma, G. Jiang, D. Margolis, J. Dumond, Y. Zhang, Silk fibers assisted long-term 3D culture of human primary urinary stem cells via inhibition of senescence-associated genes: potential use in the assessment of chronic mitochondrial toxicity, Mater Today Adv 15 (2022), 100261, https://doi.org/10.1016/j.mtadv.2022.100261.
[43] S. Hamed, B. Brenner, A. Aharon, D. Daoud, A. Roguin, Nitric oxide and superoxide dismutase modulate endothelial progenitor cell function in type 2 diabetes mellitus, Cardiovasc. Diabetol. 8 (2009) 56, https://doi.org/10.1186/1475-2840-8-56.
[44] P. Hu, N. Tirelli, Scavenging ROS: superoxide dismutase/catalase mimetics by the use of an oxidation-sensitive nanocarrier/enzyme conjugate, Bioconjugate Chem. 23 (3) (2012) 438–449, https://doi.org/10.1021/bc200449k.
[45] S.M. El-Bahr, S. Shousha, I. Albokhadaim, A. Shehab, W. Khattab, O. Ahmed-Farid, O. El-Garhy, A. Abdelgawad, M. El-Naggar, M. Moustafa, O. Badr, M. Shathele, Impact of dietary zinc oxide nanoparticles on selected serum biomarkers, lipid peroxidation and tissue gene expression of antioxidant enzymes and cytokines in Japanese quail, BMC Vet. Res. 16 (1) (2020) 349, https://doi.org/10.1186/s12917-020-02482-5.
[46] M.R. Metukuri, R. Namas, C. Gladstone, T. Clermont, B. Jefferson, D. Barclay, L. Hermus, T.R. Billiar, R. Zamora, Y. Vodovotz, Activation of latent transforming growth factor-beta1 by nitric oxide in macrophages: role of soluble guanylate cyclase and MAP kinases, Wound Repair Regen. 17 (4) (2009) 578–588, https://doi.org/10.1111/j.1524-475X.2009.00509.x.
[47] L. Liu, Z. Ding, Y. Yang, Z. Zhang, Q. Lu, D.L. Kaplan, Asiaticoside-laden silk nanofiber hydrogels to regulate inflammation and angiogenesis for scarless skin regeneration, Biomater. Sci. 9 (15) (2021) 5227–5236, https://doi.org/10.1039/d1bm00904d.
[48] Q. Dong, D. Zu, L. Kong, S. Chen, J. Yao, J. Lin, L. Lu, B. Wu, B. Fang, Construction of antibacterial nano-silver embedded bioactive hydrogel to repair infectious skin defects, Biomater. Res. 26 (1) (2022) 36, https://doi.org/10.1186/s40824-022-00281-7.
[49] L. Zhu, X. Liu, L. Du, Y. Jin, Preparation of asiaticoside-loaded coaxially electrospinning nanofibers and their effect on deep partial-thickness burn injury, Biomed. Pharmacother. 83 (2016) 33–40, https://doi.org/10.1016/j.biopha.2016.06.016.
[50] Y. Kimura, M. Sumiyoshi, K. Samukawa, N. Satake, M. Sakanaka, Facilitating action of asiaticoside at low doses on burn wound repair and its mechanism, Eur. J. Pharmacol. 584 (2–3) (2008) 415–423, https://doi.org/10.1016/j.ejphar.2008.02.036.
[51] J. Cheng, H.L. Yang, C.J. Gu, Y.K. Liu, J. Shao, R. Zhu, Y.Y. He, X.Y. Zhu, M.Q. Li, Melatonin restricts the viability and angiogenesis of vascular endothelial cells by suppressing HIF-1α/ROS/VEGF, Int. J. Mol. Med. 43 (2) (2019) 945–955, https://doi.org/10.3892/ijmm.2018.4021.
[52] H. Liu, Y. Li, J. Xiong, The role of hypoxia-inducible factor-1 alpha in renal disease, Molecules 27 (21) (2022) 7318, https://doi.org/10.3390/molecules27217318.
[53] J.A. Beamish, P. He, K. Kottke-Marchant, R.E. Marchant, Molecular regulation of contractile smooth muscle cell phenotype: implications for vascular tissue engineering, Tissue Eng., Part B 16 (5) (2010) 467–491, https://doi.org/10.1089/ten.TEB.2009.0630.
[54] K.W. Ko, B. Choi, E.Y. Kang, S.W. Shin, S.W. Baek, D.K. Han, The antagonistic effect of magnesium hydroxide particles on vascular endothelial activation induced by acidic PLGA degradation products, Biomater. Sci. 9 (3) (2021) 892–907, https://doi.org/10.1039/d0bm01656j.